Journal of Materials Science and Engineering A 3 (5) (2013) 305-314

PbS Nanostructures Thin Films by in situ PbS:Ni and PbS:Cd-Doping

Salvador Rosas Castilla[1], Marcial Zamora Tototzintle[1], Rey Baltazar López Flores[2], Leslie Chaltel Lima[1] and Oscar Portillo Moreno[1]

1. Faculty of Chemistry, Autonomous University of Puebla (UAP), Puebla, Mexico

2. Faculty of Electronics, Autonomous University of Puebla (UAP), Puebla, Mexico

Received: November 16, 2012 / Accepted: December 07, 2012 / Published: May 10, 2013.

Abstract: PbS:Ni and PbS:Cd nanocrystalline films were prepared by chemical bath on glass substrates at deposition T = 80. Different Ni-Cd-doping levels were obtained changing the volume of the Ni an Cd-reagent-solution into the PbS growing solution. Measurements were carried out to characterize the semiconductor,such as X-ray diffraction (XRD) and optical absorption (OA). The morphological changes of the layers were analyzed using scanning electron microscopy (SEM). Diffraction X-ray spectra PbS:Ni and PbS:Cd displayed peaks at 2θ = 26.00, 30.07, 43.10, 51.00 and 53.48, indicating growth on the zinc blende face. The grain size determined by X-rays diffraction of the undoped samples, was found ~37 nm, whereas with the doped sample was 32-5 nm. PbS: Ni forbidden band gap energy (E_g) shift disclose a shift in the range of 1.4-2.4 V and PbS:Cd energy was estimated to be 0.15-0.5 eV. Gibbs free energy calculation for the Cu doping PbS is also included.

Keywords: Thin films, nanocrystals, potential cell, quantum confinement effect, coordination complex.

1. Introduction

The ever-increasing interest into deposition of ternary derivative materials, the potential of designing and tailoring both of the lattice parameters and the forbidden band-gap energy (E_g) by controlling growth parameters [1] is very huge. In this regard, many techniques have been successfully employed: vacuum evaporated [2], sol gel methods [3], etc.. Most of the studies reported so far have focused in the deposition of ternary derivatives material in thin films as $Cd_{1-x}Fe_xS$ [4], $Cd_{1-x}SCu_x$ [5] and $Pb_{1-x}Ni_xS$ [6]. Noteworthy is the fact that PbS thin films are promising photovoltaic materials as their variable E_g can be adjusted to match the ideal ~1.5 eV required for achieving a most efficient solar cell [7], likewise size-dependent new physical aspects have generated an ongoing thrust for new practical applications and PbS nanocrystals with grain-size (GS) dimensions in the range of 1-20 nm are of technological interest for advanced optoelectronic applications, showing a stronger quantum confinement effect when the crystallite size matches the dimension of Bohr exciton [8]. In this context, there are two situations, called the weak confinement and the strong regimes [9, 10]. In the weak regime, the particle radius of the electron-hole pair, but the range of motion of the exciton is limited, which causes a blue shift in the absorption spectrum. When the size of the nanoparticles are below Bohr radius, its lead to the quantum confinement effect. This confinement induces discrete electronic states in the valence and conduction band of the quantum dots compared to the continuous state of energy in bulk material. If the crystallite size is below the exciton Bohr of the semiconductor, strong quantum confinement occurs. The confinement effect appears as a shift in absorption spectra and the absorption to lower wavelengths,

Corresponding author: Oscar Portillo Moreno, Ph.D., professor, research field: materials. E-mail: osporti@yahoo.com.mx.

wicks is due to change in the E_g [11] and control over assembly through modification of surface functionalization. On the other hand, photovoltaic devices are an widely recognized potential application for nanocrystals due, in part, to their high photoconductivity, easy work-up for solutions and also low cost of production. In this regard, growing interest has been devoted to the Pb-chalcogenide family for nanocrystals solar cell applications because they have such large exciton Bohr radii of 18 nm, in the limit where the nanocrystals are only a tenth part or so of the bulk exciton diameter: electrons and holes can then tunnel through a thin surface coating, and therefore strong electronic coupling between particles allows the transport of charge between nanocrystals. It must be pointed out that the synthesis of ternary $Pb_{1-x}Ni_xS$ nanocrystals remains largely underdeveloped compared to the widely studied cadmium chalcogenide. Thus, on this frame of reference, in the present work attempt prepared PbS Ni^{2+} and Cd^{2+} doped nanostructured films by chemical bath (CB), in order to investigate structural and optical of undoped and doped-PbS films. Surface morphology and composition were determined using a Carl Zeiss Auriga 39-16 coupled with a Bruker energy dispersive analysis of X-rays (EDAX). The crystalline structure characterization was carried out by XRD patterns registered in a D8 Discover diffractometer, using the Cu K_α line. The grain size was determined utilizing the Scherers formula on XRD patterns. The optical absorption spectra, measured employing a Unicam 8700 Spectrometer, allow to calculate the forbidden band gap energy (E_g) by using the $(\alpha h\nu)^2$vs. $h\nu$ plot, where α is the optical absorption coefficient and $h\nu$ the photon energy.

2. Chemical Reactions and Experimental Procedure

The reactions for the growth of PbS films doped with Ni^{2+} and Cd^{2+} were determined by employing the cell potential values in basic media reported [12]. The cell potential and the Gibbs free energy are related through the Nernst equations: $\Delta G^o = - n\tau\varepsilon^o$, where n is the number of equivalents, τ is the Faraday constants and ε^o are the cell potential, ΔG^o is calculated for the reaction. Value ΔG^o provides thermodynamic information on the spontaneity of chemical reactions. Worth-noting is the formation of the coordination complex $[M(NH_3)_4]^{2+}$, which is determinant for the release of M^{2+} ions (M^{2+} = Cd^{2+}, Pb^{2+}, Zn^{2+}, etc.) and their slow recombination with S^{2-} ions that, under these conditions, leads to the spontaneous formations to the MS precipitate in an easily controlled process. The growth of PbS is therefore carried out according to the following steps: (a) by mixing $Pb(CH_3CO_3)_2$, KOH and NH_4NO_3, the coordination complex $[Pb(NH_3)_4]^2$ is generated indirectly; (b) The S^{2-}ions are found in the solution and are generated by the thiourea decomposition in alkaline solution; (c) The aforementioned steps allow the slow process at the substrate surface to take place predominantly over direct hydrolysis of thiourea in the bulk of the reaction bath as follow [13, 14]:

$$SC(NH_2)_2 + 3OH^- \Leftrightarrow CO_3^{2-} + S^{2-} + NH_4^+ + \frac{1}{2}O_2 \quad (1)$$

$$[Pb(NH_3)_4]^{2+} + Pb + S^{2-} \Leftrightarrow PbS + Pb^{2+} + 4NH_3, \Delta G^o = +335.48 \text{ KJ} \quad (2)$$

$$[Pb(NH_3)_4]^{2+} + H_2S + S^{2-} \Leftrightarrow PbS + 4NH_3 + S + 2H^+ + 2e, \ \Delta G^0 = +362.88 \text{ KJ} \quad (3)$$

$$HPbO^- + H_2O + [Pb(NH_3)_4]^{2+} + H_2S + S^{2-} \Leftrightarrow PbS + 4NH_3 + S + 2H^+ + Pb + OH^- + Pb^{2+} \quad (4)$$

$$Pb + 2S^{2-} + Ni(OH)_2 \Leftrightarrow PbS + HS^- + Ni^{2+} + OH^-, \Delta G^0 = -29.79 \text{ KJ} \quad (5)$$

$$Cd(OH)_2 + 2e \Leftrightarrow Cd + 2OH^-, \ \Delta G^0 = -156.13 \text{ KJ} \quad (6)$$

Since $\Delta G^o > 0$, and as such, the reaction is not a spontaneous process. Based on the Gibbs free energy values obtained from the thermodynamic equilibrium analysis, the Ni^{2+} and Cd^{2+} ionization state probably is present in the volume of PbS under our work conditions comparing the changes in ΔG^0, which thermodynamically enable to the growth of the PbS:Ni^{2+} and PbS:Cd^{2+}. Deposition includes different

limiting physical and chemical processes which determine the kinetic behaviour of the doped PbS: (1) nucleation stage. It is the initial stage requiring a high activation energy in which reactive centres (nuclei) are formed on the surface on the substrate; (2) growth stage. It is the second stage, which is characterized by an enhanced rate of PbS deposition; (3) doped stage. The high rate of deposition is associated with the addition level of doping, whit the accelerated growth of PbS doped nuclei formed on the substrate during the nucleation stage; (4) termination stage. During this stage, the rate of deposition gradually slows daw. This is probably due to a depletion of the reagents in deposition mixture.

The glass substrates were previously immersed in a $K_2Cr_2O_7$/HCl/H_2O solution for 24 h, after which they were rinsed in deionised water and dried in a clean hot-air flow. Preparation of polycrystalline PbSNi thin films on glass substrates was performed at a temperature of 80 ± 2 °C grown by chemical bath (CB) and pH = 11.0. The growth of PbS films with six different levels of doping V[Ni^{2+}] were obtained by the addition in situ: 2, 4, 6, 8, 10 and 12 mL in the solutions for PbS growth $Pb(COOH)_2$ (0.01 M), KOH (0.5 M), NH_4NO_3 (1.5 M), $SC(NH_2)_2$ (0.2 M). The solutions were mixed and the final solution heated at 80 ± 2 °C during 2 h, with the substrate remaining inside the solution. The optimal concentration of the doping solution V[Ni^{2+}], $Ni(NO_3)_2$ (0.023 M) was determined after several trials, until films had attained good adherence. This solution is routinely added to the reaction mixture during the growth of the PbS films. The samples were labelled as PbSNi0 for the undoped sample, PbSNi2-PbSNi10 for the doped samples [6]. The total volume of the growing-solution consisted of the volume-solution (V_{PbS}) for the PbS growth plus the volume-solution V[Ni^{2+}] containing the doping Ni^{2+} chemical agent: V_{PbS} + V[N^{i2+}] = V_{tot}. The relative volume V[Ni^{2+}] changed from 2 to 12. The films were growing obtained were silver-colored, polycrystalline reflective, with a homogeneous consistency and good adhesion to the substrate.

PbSCd thin films on substrates on glass substrates at 80 ± 2 °C grown by chemical bath CB and pH = 11.0. We growth PbSCd films with five different levels of doping Cd^{2+}: 2, 4, 6, 8, 10 mL. The solutions used for the deposit of PbS are: 0.01 M $Pb(COOH)_2Pb$, 0.5 M KOH, 1.5 M NH_4NO_3, 0.2 M $SC(NH_2)_2$ and the doping solution was $CdCl_2$ at optimal concentration 0.02 M. The growth PbSCd films with five different levels of doping $V_{[Cd^{2+}]}$ were obtained by the addition in situ: 2, 4, 6, 8, 10 mL in the solutions for PbS growth [15]. This solution is routinely added to the mixture of the reaction during the growth of the PbS film. All the solutions used were prepared with deionised water of resistivity 18.2 MΩ.

3. Results

3.1 Electron Dispersion Spectroscopy (EDAX)

The semi-quantitative analysis of the films was carried out by using the EDAX technique for undoped and doped PbSCd and PbSNi thin films at different points to study the stoichiometry of the films. In Table 1 are displayed the atomic concentrations of Pb, S and Cd obtained fromscanning electron spectroscopy (SEM) [15].

The morphological analysis of the PbSCd films was carried out in scanning electron microscopy (SEM). Micrographs are show in Fig.1:(a) micrographs of the films undoped, (b) doped with 6 mL, (c) doped with 10 mL. You can see the uniform surface morphology, which is compact and polycrystalline. The SEM micrographs show that the particle grain size decreases with Cd^{2+} concentration. The granules are made of different sizes; we can conclude that the doping plays a vital role on the properties of the PbSCd thin films. The micrographs of the films with doping levels of 2, 4 and 8 mL, are not shown. The these micrographs are appreciated for the films which undoped, and which have compactly highly reflective characteristics of the PbS obtained by means of the

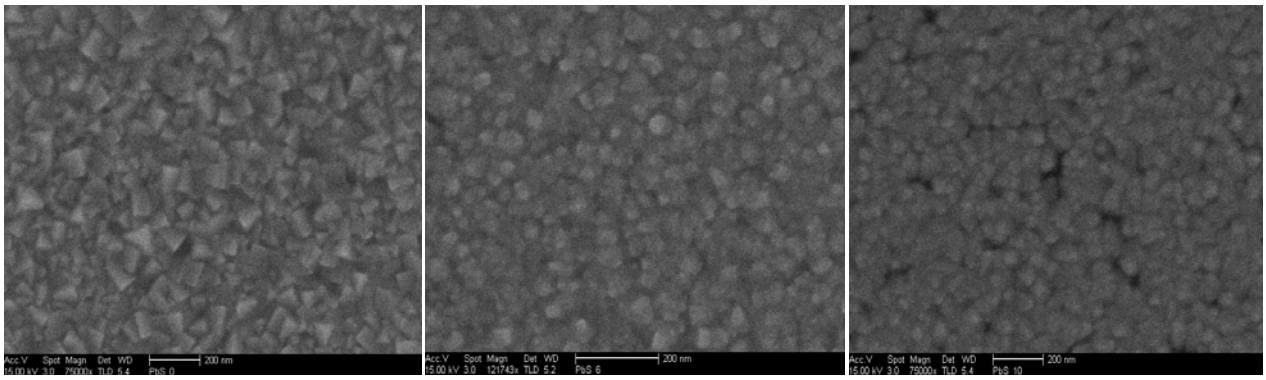

(a) (b) (c)

Fig. 1 Micrographs of the films: (a) undoped PbSCd0; (b) doped 6 mL PbSCd6; (c) doped 10 mL PbSCd10.

technique CB [16], and those that doped have crystals in the form of spheres. A very adherent film with gray-black colour metallic aspect was obtained in case of a undoped and doping PbS films reveal a continuous compact polycrystalline films with similar morphology have been reported [17].

It is displayed in Table 1, the atomic concentrations of Pb, S and Ni by PbS:Ni^{2+} films.

For the samples the increase in concentration of Ni in PbS films is easily noted, reaching a percent value of Ni = 11.51. In this case, when Ni^{2+} ionenters as a substituteofthe Pb^{2+} ion, it is observed that the sample was slightly deficient in S^{2-} ion.

Therefore, for the higher V[Ni^{2+}] values considered, growth material can probably be estimated as doped semiconductor but actually the material canberegarded as similar to a solid solution of $Pb_{1-x}Ni_xS$.

Table 1 Atomic concentrations of Pb, S and Cd obtained from EDAX.

	Atomic concentrations (%)		
Sample	Pb	S	Cd
PbSCd0	56.35	43.05	0.0
PbSCd6	60.10	18.38	21.51
PbSCd10	56.29	33.49	10.22

Table 2 Atomic concentrations of Pb, S and Ni obtained from EDAX.

	Atomic concentrations		
Sample	Pb	S	Ni
PbS-Ni0	56.35	43.05	0.0
PbS-Ni6	70.10	18.38	11.51
PbS-Ni12	56.29	33.49	10.22

In this case, when Ni^{2+} ion enters as substitute of the Pb^{2+} ion, probably for the higher $V_{[Ni2+]}$ values considered here the growth material can also be estimated as a doped semiconductor being the material also as in the aforementioned conditions, similar to a solid solution of $Pb_{1-x}Ni_xS$ [6, 15]. The micrographs of undoped- and doped-PbS films are showed in Fig. 2. Scale bar at 1.0 μm and 30 nm, respectively were obtained from SEM. The undoped-PbS0Ni, doped-PbSNi6 (6mL), doped-PbS12Ni (12mL) films are showed. As can be seen from the uniform surface morphology, such aspect is compact and of polycrystalline nature. The SEM micrographs show that the particle grain size decreases with an increase in V[Ni^{2+}] concentration and granules appeared to be of different sizes. In such micrographs for the undoped films, crystals as small spheres are observed. A very adherent film with metallic gray-black colored aspect was obtained for undoped and doped films revealing continuous and compact polycrystalline films. Similar morphologies have been reported [17].

3.2 X-Ray Diffraction (XRD)

Fig. 3 shows sample diffractograms of X-ray PbSCd films. These spectra of X-ray, show peaks located at the following angular positions: 2θ = 26.00, 30.07, 43.10, 51.00 and 53.48. Diffraction along the (111) plane shows the highest intensity well-defined sharp peak, indicated high crystallinity of the material prepared.

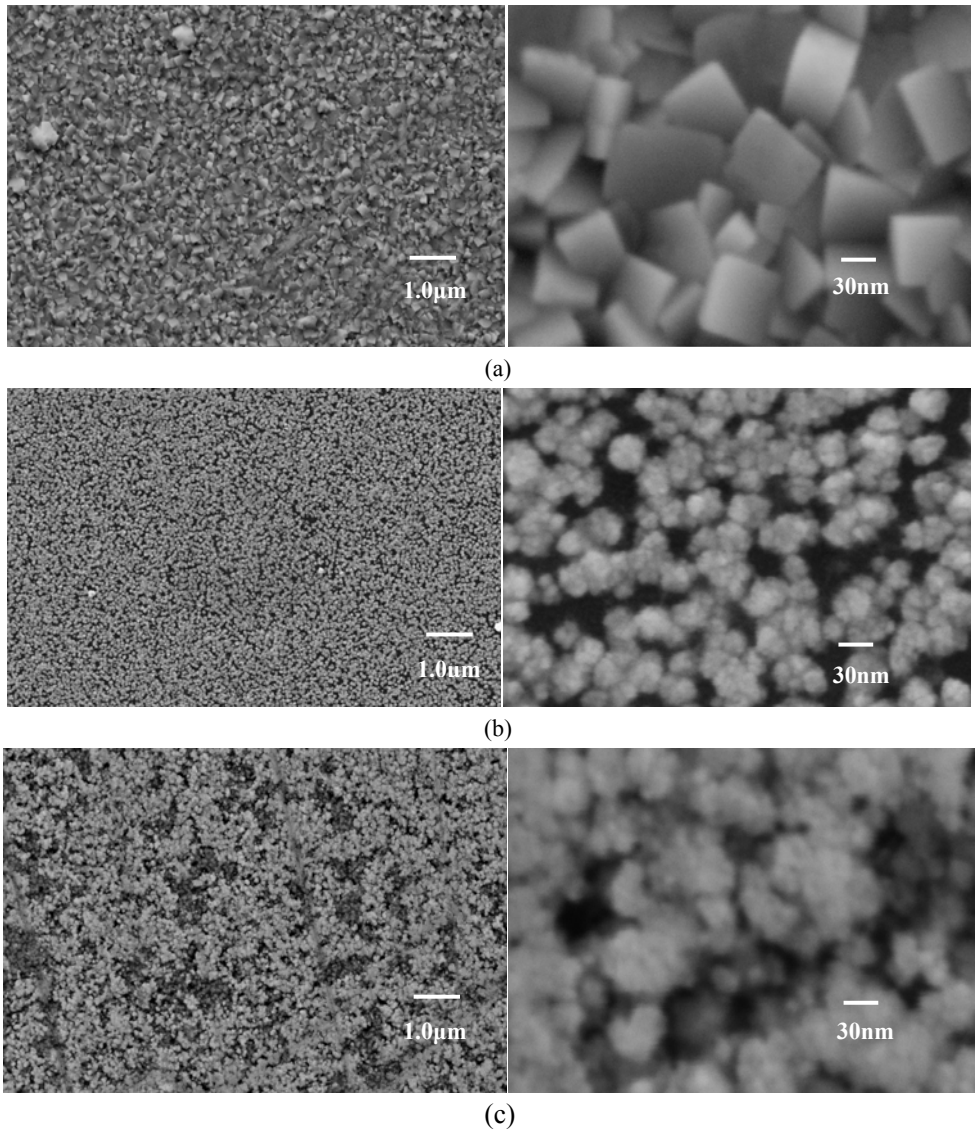

Fig. 2 Micrographs obtained from SEM of the films with scales of 1.0 μm and 30 nm for: (a) undoped-PbSNi0; (b) PbSNi6; and (c) PbSNi12-films.

These belong to the wurzite phase according to reference patterns JCPDS 05-0592. The spectrum of films PbSCd4, shows two peaks located in the angular positions 2θ = 27.25 and 28.49, which belong to the PbO in monoclinic phase, according to the standards JCPDS 019-0697, another peak in 2θ = 34.04, which corresponds to PbO in orthorhombic phase according to the standards JCPDS 052-0772. The growth of the PbO was favored according to the following reaction:

$$PbO_3^{2-} + H_2O + 2e \Leftrightarrow PbO + 2OH^-$$

Pentia et al. [17] proposed the formation of PbO as a process of absorption according to the following reaction:

$$PbO + 2OH^- \Leftrightarrow PbO + H_2O + 2e,\ \Delta G^0 = +111.94\ KJ \quad (7)$$

However, in our work, we only generate this oxide in PbSCd4 sample. Other authors using the spray pyrolysis identified mix of phase control of the mole fraction x getting a solid solution of $(CdO)_{1-x}(PbO)_x$ [18], is exhibited the average grain size (GS) of PbS for the sample that was undoped and the doped one corresponding to the (111) plane against the volume of the doping (Fig. 4). For the PbSCd8 film can be seen GS ~29 nm. In this plot, it is possible to be seen

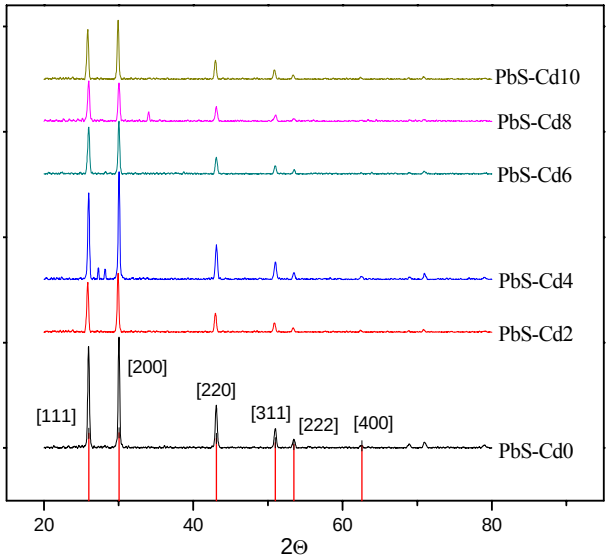

Fig. 3 XRD patterns of the undoped and PbS doped Cd^{2+} films. From V = 0 to V = 10 the patterns are placed consecutively.

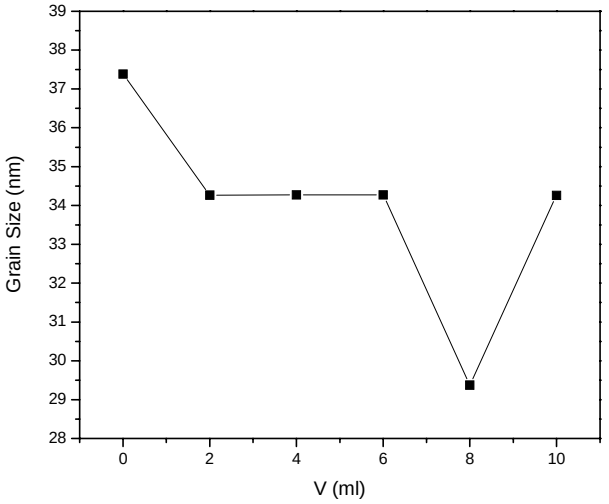

Fig. 4 Average grain size, calculated from the width of the main peak of the XRD patterns vs. volume doping in the (111) crystalline plane.

that the GS decreases for the sample PbSCd2 and remains without change for 4, 6, 10 mL at 34 nm [15].

The effect of the decrease of the GS by the effect of the doping has been reported in CdS films doped Cu^{2+} by CB [5]. A possible explanation to this experimental fact can be given as it follows: The ionic radii data are Pb^{+2} = 1.21 Å, S^{2-} = 1.84 Å and Cd^{2+} = 0.95 Å, for relative low concentration Cd^{2+} ions can be majority situated in (1) Pb^{2+} vacancies sites which otherwise would be empty, (2) in Pb^{2+} sites provoking the appearing in Pb interstitial, and (3) in interstitial positions. At this level of Cd^{2+} the PbS can be considered a doped material. That tendency to amorphize the material makes the localized monocrystalline zones (grains) become smaller and smaller as Cd^{2+} increases, growth nanocrystals. The dimensions of the crystallites depend on the experimental parameters namely pH, concentrations of reactants, temperature, substrate and doping. In this work, adding to the starting solution a small quantity of doping changes in a crystallites order and/or alteration of their size can be observed. A decrease in the degree of the order of crystallites, this is expected to lead to enhanced growth of stable nuclei in the initial stages of growth followed by impaired grain growth, hence, resulting in smaller grains in the cadmium.

Fig. 5 shows diffractograms of X-ray (XRD) PbSNi films. Such X-ray spectra display peaks located at the following angular positions: 2θ = 26.00, 30.07, 43.10, 51.00 and 53.48. They are related with the reflection peaks of (111), (200), (220), (311), (222), respectively, and all these diffraction peaks can be perfectly indexed to diffractograms PbS samples displaying the zinc-blende (ZB) crystalline phase according to reference patterns JCPDS 05-0592. The XRD spectra

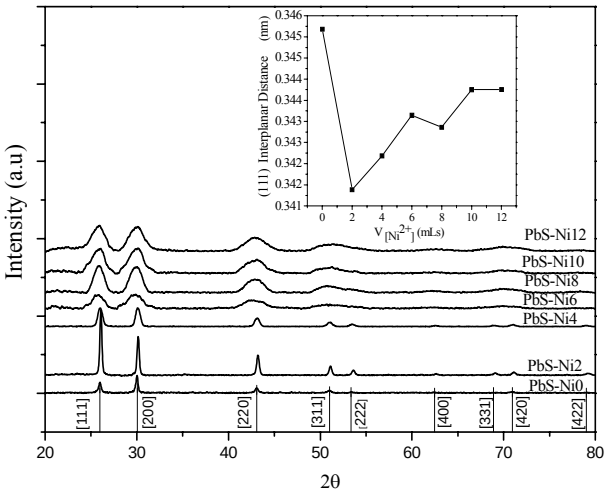

Fig. 5 XRD diffractograms PbS:Ni films. The patterns are placed consecutively. The inset illustrates the (111) reflections of the cubic phase as function of V[Ni^{2+}].

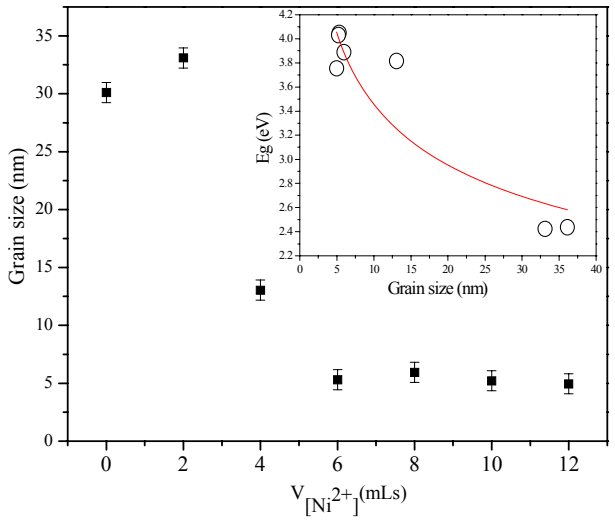

Fig. 6 The average grain size (GS) with of the mean peak of XRD patterns vs. V[Ni^{2+}]. The inset exhibits the E_g vs. GS plot.

for PbSNi2 films indicate that (111) is the orientation of PbSNi grains; the PbSNi2 diffraction layer along the (111) plane reveals the highest intensity of a well-defined sharp peak, indicating the high crystallinity of the obtainedmaterial [6].

The intensities for PbSNi2 and PbSNi4 layers for (111), (200) and (220) are nearly equal and all the representative diffraction lines of PbS can be observed. In the PbSNi2 film, the (111) reflection has the highest intensity. This phenomenon may be attributed to the doping effect. The low intensity peaks observed in the XRD patterns of the doped PbSNi6 to PbSNi12 samples indicates that the films are coarsely fine crystallites or nanocrystalline. The broad hump in the displayed pattern is due to an amorphous glass substrate and also possibly due to some amorphous phase present in the PbSNi crystallite size of films. These effect are associated with the nanocrystals doped-PbSNi with V[Ni^{2+}] in the regime were the cluster mechanism is dominating (on the contrary to films grown via ion-ion mechanism, the crystal size was larger), and consist of PbSNi nanocrystals embedded in an apparent matrix of PbS. The inset in Fig. 5 displays the (111) interplanar distance (ID) for the ZB face, calculated from the 2θ peak positions, vs. V[Ni^{2+}]. This ID is close to the (111) ID of the ZB phase. First, the ID decreased with V[Ni^{2+}]due to the presence of Ni^{2+} in substitution sites and, finally, reaching a maximum value in PbSNi6 film.The ionic radii data are Ni^{2+} = 0.69 Å, therefore for a relative low concentration of Ni^{2+} ions a majority can be located in: (1) Pb^{2+} vacancies sites, which otherwise would be empty; (2) in Pb^{2+} sites causing the appearance of Pb interstitial, and (3) in interstitial positions. At this level of V[Ni^{2+}], the PbSNi can be considered a doped material [6]. The incorporation of Ni^{2+} solubility has been proven to be more effective in Pb chalcogenide than Zn-chalcogenide, a result explained in terms of the cation size. The effect of the GS decrease by the doping effect has been reported in films of CdS doped with Cu^{2+} by CB [6]. A decrease in the degree of the order of crystallites is expected to lead to enhanced growth of stable nuclei at the initial stages of growth, followed by impaired grain growth, and hence resulting in smaller grains in the nickel. In the inset of Fig. 6, E_g is displayed as function of the GS. For low GS, E_g increase, as GS decreases, E_g increase. When GS ≅ 5 nm, E_g reaches a maximum value. For a larger GS, E_g decreases. Two effects can be considered in such E_g changes: (1) The variation of ID, and (2) the strong quantum confinement.

3.3 Optical Absorption (OA)

Assuming parabolic band structure, the absorption coefficient α is proportional to:

$$\left(E - E_g\right)^{\frac{1}{2}} = \alpha h\gamma \tag{8}$$

And an extrapolation to $\alpha^2 = 0$ yields a good approximation of the energy gap E_g [19, 20]. The optical property of materials information is obtained using the technique. With this technique it is possible to plot the percentage (%) of the transmittance vs. the wavelength (λ), and by using the Planck equation $E = hc/\lambda$, the energy of the incident photon for each value of the wavelength of light is expressed in terms of the energy of the photon incident in this way is the spectra

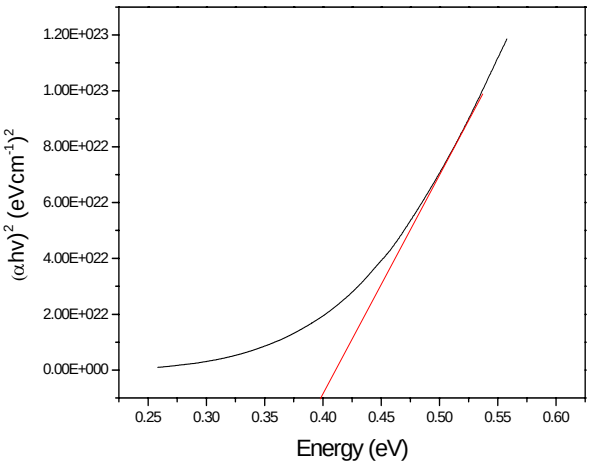

(a)

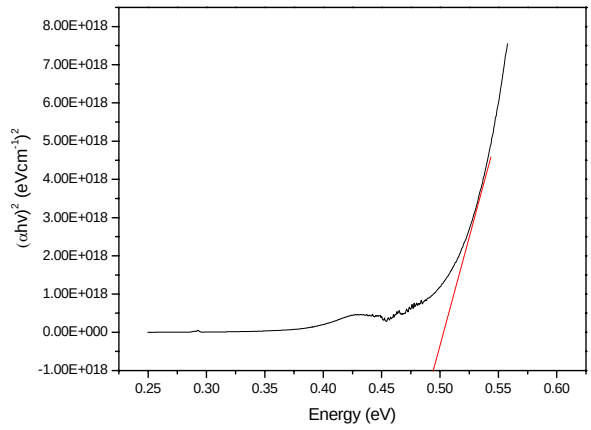

(b)

Fig. 7 Optical Absorption spectra for the sample (a) PbSCd0 and (b) PbSCd10.

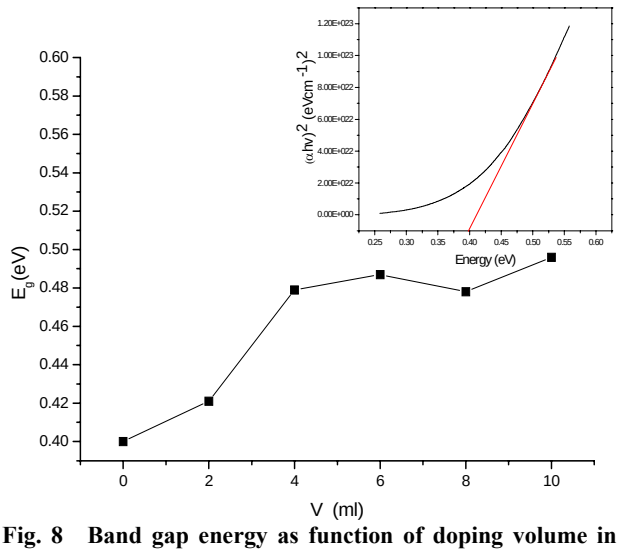

Fig. 8 Band gap energy as function of doping volume in the range 0.25-0.60 eV, PbSCd, the inset illustrates the method to calculate from optical absorption measurements.

of (%) of T vs. the energy of the incident photon and where $T + R = 100$, where T is the transmittance and R the reflectivity of the film. Fig. 7 shows the spectra of the optical absorption for the samples: (a) PbSCd0 and (b) PbSCd10. The fundamental absorption which corresponds to electron excitation from the valence band to conduction band can be used to determine the nature and value of optical band gap. For the simple PbSCd0, through the intersection of the straight line with the axis of the photon energy is obtained E_g = 0.40 eV and in a similar way to the sample PbSCd10 E_g = 0.51 eV.

The Fig. 8 shows E_g vs. the doping and the upper right part of the same plot shows the spectrum of absorption for the sample undoping. In this plot, it can be observed that the sample of PbSCd2: E_g = 0.34 eV. The shift experimentally observed E_g valuesindicated alloying between nanocrystalline PbS and CdS phases. The Fig. 9 illustrates the forbidden band gap the layers in range of 2.2-3.0 eV, the large experimentally observed E_g in the nanoparticle films to theorically estimated (using Vegar's law) E_g for bulk shows the extent of quantum size effect in nanoparticle films. It can be seen that size effect on the optical band gap is stronger nanoparticle films than in PbS nanoparticles of 24 nm, which is 3.4 times than the E_g for bulk PbS

Fig. 9 shows a graph of E_g vs. $V_{[Ni^{2+}]}$ and in the inferior right part the plot shows the absorption spectrum for the sample PbSNi12. In this plot, it can be observed a E_g = 2.4 eV value for the PbSNi0 sample. The confinement effect appears as a shift in edge of the absorption spectra and the absorption to lower wavelengths, possibly due to the decrease in GS, the decrease in number of defects and the change in color. It is clearly seen from the optical spectrum an absorption edge shift toward a lower wavelength in doped films. The experimentally observed E_g values for the shift indicated an alloying between nanocrystalline PbS. Such increase has been observed by other authors [8, 21]. The E_g for doped samples in the 2.4-3.8 eV range the large experimentally

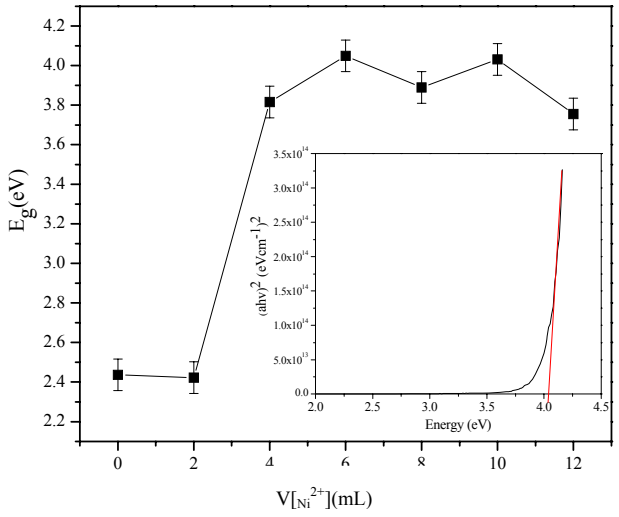

Fig. 9 Band gap energy as function of doping volume in the range 2.2-4.0 eV, PbSNi, the inset illustrates the method to calculate from optical absorption measurements.

observed E_g in the nanoparticle films theoretically estimated (using Vegar's law) E_g for bulk shows the extent of quantum size effect in the nanoparticle films. The fundamental optical transition of doped films (E_g = 0.41 eV) is not observed in these films, presumably because of complete mixing of PbS with Ni^{2+} affording an unique ternary intermetallic compound of the $Pb_xNi_{1-x}S$ type. It is observed that the size effect on the optical band gap is stronger in nanoparticle films than in PbS nanoparticle of 24-10 nm (average crystallite size) and show an E_g: 2.22-2.65 eV. The observed increase in the quantum size effect could possibly be attributed to a decrease in the effective mass. The increased in E_g when increasing the concentration of $V[Ni^{2+}]$ in the films is reflected by the presence of an excitonic structure material. Excitonic structures are readily observed in large E_g semiconductors with binding energy such as CdSe [10].

The E_g optical doped films varied from 2.4-3.8 eV, with doping increase of $V[Ni^{2+}]$. A similar shift observed in the position of the excitonic peak towards higher energies in CdSe crystallites has been explained due to a decrease in crystallite size [22]. The red shift of the band gap is associated with the decline of the SG. It is clear that the E_g increase when $V[Ni^{2+}]$ increases. As mentioned earlier, we observed a systematic decrease in the crystallite size with increasing concentration. Since the estimated mean crystallite size in this case being approximately half the value of the exciton Bohr radius in PbS, we observe a strong confinement in doped PbSNi films.

4. Conclusions

We have reported the growth of doped-PbS with Cd^{2+} and Ni^{2+} ions affording nanocrystalline films by the chemical bath technique. X-ray spectra show 2θ = 26.00, 30.07, 43.10, 51.00 and 53.48, which belong to the ZB phase in two layers. The GS lies in the interval of ~32-5 nm for PbSNi. The E_g of films increased from 2.4-3.8 eV when doping $V[Ni^{2+}]$ is increased. GS reduces in the interval 2 mL ≤ $V[Ni^{2+}]$ ≤12 mL and a E_g increase as function of the GS is displayed. When GS ≅ 5 nm. The XRD PbSCd4 films show two peaks which are located in the angular position at 2θ = 27.25 and 28.49, which belong to the PbO in a monoclinic phase and another peak in 2θ = 34.04, which corresponds to PbO in an orthorhombic phase. Optical absorption spectra is quantified for the film PbSCd10 film which is undoped, and it happens to be E_g 0.4-0.51 eV. The optical band gap PbSNi films varied from 2.1-4.0 eV, increase doping Ni^{2+}. We deem two effects occur on E_g changes: (1) The variation of ID, and (2) the quantum confinement.

Acknowledgments

The authors thank to Lic. Damián Hernández Méndez, principal of Attention and Management University of the Benemérita Universidad Autónoma de Puebla, México.

References

[1] N.S. Kozhevnikova, A.A. Rempel, F. Hergert, A. Mageruli, Structural study of the initial grow of nanocrystalline CdS thin films, Thin Solid Films 517 (2009) 2586-2589.

[2] S. Kumar, T.P. Sharma, M. Zulfequar, M. Husain, Characterization of vacuum evaporated PbS films,

Physica B 325 (2003) 8-16.

[3] A. Sashchiuk, E. Lifshitz, Optical and conductivity properties of PbS nanocrystals amorphous zirconia sol-gel films, Journal of Sol-Gel Science and Technology 24 (2002) 31-38.

[4] X.J. Wu, D.Z. Shen, Z.Z. Zhang, J.Y. Zhang, K.W. Liu, B.H. Lu, et al., p-Type conductivity and donor-acceptor pair emission in $Cd_{1-x}Fe_xS$ diluted magnetic semiconductors, Appl. Phys. Lett. 89 (2006) 262118-262121.

[5] O.P. Moreno, H.L. Lima, V.R. Falcón, J.M. Juárez, G.J. Díaz, R.L. Morales, et al., Growth of CdS:Cu nanocrystals by chemical synthesis, J. Electrochem. Soc. 153 (2006) 926.

[6] M.C. Portillo, J.M. Juárez, G.A. Ávila, M.Z. Tototzintle, M.M. Barragán, J.R. Cerna, et al., Growth of PbS:Ni nanocrystals thin films by chemical bath, Journal of Materials Science and Engineering A (2) 5 (2012) 410-422.

[7] W.L. Ma, J.M. Luther, H. Zheng, Y. Wu, A.P. Alivisatos, Photovoltaic's devices employing ternary PbS_xSe_{1-x} nanocrystals, Nanoletters 518 (2010) 3164-3168.

[8] A.S. Obaid, M.A. Mahdi, Z. Hassan, M. Bououdina, Characterization of nanocrystalline PbS thin films prepared using microwave-assisted chemical bath deposition, Materials Science in Semiconductors Processing 15 (2012) 564-571.

[9] S. Thangavel, S. Ganesan, S. Chandramohan, P. Sudhgar, Y.S. Kang, C.H. Hong, Band gap engineering in PbS nanostructured thin films from near-infrared dawn to visible range by in situ Cd doping, Journal of Alloys and Compounds 495 (2010) 234-237.

[10] A.R. Márquez, M.R. Falfán, R.L. Morales, O.P. Moreno, O.P. Moreno, O.Z. Ángel, et al., Quantum confinement and crystalline estructure of CdSe nanocrystalline films, Phys. Stat. Sol. 188 (2001) 1059-1063.

[11] S. Seghaier, N. Kamoun, R. Brini, A.B. Amara, Structural and optical properties of PbS thin films deposited by chemical bath deposition, Material Chemistry and Physics 97 (2006) 71-80.

[12] A.J. Bethune, N.A.S. Loud, Standard aqueous potential an temperature coefficients at 25 °C, Skokie 2 (1969) 107-108.

[13] O.P. Moreno, G.A. Avila, J.R. Cerna, J.H. Tecorralco, M.C. Portillo, R.L. Morales, et al., Characterization of chemical bath deposited CdS, CdSe and PbS, Journal of Materials and Engineering A 1 (2011) 692.

[14] O.P. Moreno, H.L. Lima, R.L. Morales, R.P. Merino, O.Z. Ángel, $Cd[_{S(1-x)} + CO_{3(x)}]$ thin films by chemical bath synthesis, Journal of Materials Science 40 (2005) 1-4.

[15] O.P. Moreno, M.C. Portillo, M.M. Flores, J.M. Juarez, G.A. Avila, R.L. Morales, et al., Properties of chemical bath deposited PbS thin films doped with Cd^{2+}, Journal of Materials Science and Engineering A 1 (211) 759-767.

[16] A. Popa, M. Lisca, V. Stancu, M. Buda, E. Pentia, T. Botilae, Crystallite effect in thin film PbS grown on glass substrates by chemical bath deposition, Journal of Electronics and Advanced Materials18 (2006) 43-45.

[17] E. Pentia, L. Pintillie, T. Botila, I. Pentille, A. Chaparro, C. Maffiotte, Biinfluence on growth and physical properties of chemical deposited PbS films, Thin Films 434 (2003) 162-170.

[18] V.K. Kumar, K. Ramamurthi, E. Elagovan, Preparation of $(CdO)_{1-x}(PbO)_x$ and $(CdS)_{1-x}(PbS)_x$ thin films by spray pyrolysis technique and their characterization, Solid State Communications 132 (2004) 162673-162677.

[19] B. Thangaraju, P. Kaliannan, Optical and structural studies on spray deposited α-PbO thin films, Semicond. Sci. Technol. 15 (2000) 542-544.

[20] R. Swanepoel, Determination of the thickness and optical constants of amorphous silicon, J. Phys. E 16 (1983) 1214-1216.

[21] R.S. Kane, R.E. Cohen, R. Skbey, Synthesis of PbS nanoclosters within block copolymer nanoreactors, Chem. Mater. 8 (1996) 1919-1924.

[22] I. Balberg, E. Shavir, Y. Dover, O.P. Moreno, R.P. Morales, O.Z. Angel, Meyer-Neldel-like manifestation of the quantum confinement effect in solid ensembles of semiconductors quantum dots, Physical Review B 75 (2007) 1-4.